BIOCHEMISTRY
including biophysical chemistry & molecular biology

Article

pubs.acs.org/biochemistry

Kinetics and Thermodynamics of DNA, RNA, and Hybrid Duplex Formation

Brittany Rauzan, Elizabeth McMichael, Rachel Cave, Lesley R. Sevcik, Kara Ostrosky, Elisabeth Whitman, Rachel Stegemann, Audra L. Sinclair, Martin J. Serra, and Alice A. Deckert*

Department of Chemistry, Allegheny College, 520 North Main Street, Meadville, Pennsylvania 16335, United States

ABSTRACT: The rates of duplex formation for two octamers of DNA (5′ d-CACGGCTC/5′ d-GAGCCGTG and 5′ d-CACAGCAC/5′ d-GTGCTGTG), the homologous RNA, and both sets of hybrids in 1 M NaCl buffer have been measured using stopped-flow spectroscopy. In addition, the thermodynamic parameters, ΔH° and ΔS°, have been determined for the same sequences under the same buffer conditions using optical melting techniques. These data reveal a linear free energy relationship between the free energy of activation for denaturation and the change in free energy for formation of the duplexes. This relationship indicates that these duplex formation reactions occur through a common unstructured transition state that is more similar to the single strands in solution than to the ensuing duplex. In addition, these data confirm that the greater stability of RNA duplexes relative to that of homologous DNA and hybrid duplexes is controlled by the denaturation rate and not the duplex formation rate.

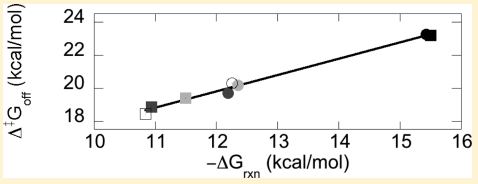

Duplex formation of nucleic acids is one of the most fundamental biological processes. RNA primers form a duplex with the parental strand DNA during replication.[1] Codon versus anticodon recognition requires the formation of a short stretch of duplex during translation.[2] SiRNAs, miRNAs, and piwiRNAs all form duplexes with their target sequences.[3−5] In addition, laboratory techniques such as polymerase chain reaction rely on duplex formation to complete a round of amplification. Therefore, understanding the molecular details of duplex formation will greatly facilitate our understanding of many processes central to the biology of the cell.

The stability of nucleic acid duplexes has been investigated by multiple laboratories.[6−11] These results have led to the development of the nearest-neighbor model for predicting the stability of nucleic acid duplexes that takes into account the strength of H-bonding and base-stacking interactions. While there is some sequence specificity, in general RNA duplexes have been found to be more stable than either the DNA or DNA−RNA hybrid duplexes with similar sequences.[6−8] These models can generally predict the stability of duplexes to within approximately 0.5 kcal/mol or within a 2-fold range of the binding constant, but the underlying reason for the relative stability of the RNA duplexes is not well understood.

A full understanding of the relative stability of homologous RNA and DNA duplexes can be obtained only by measuring both the equilibrium and kinetic parameters for the duplex formation equilibria under the same solvent conditions. Several early studies of the kinetics of duplex formation have led investigators to speculate that the stability of nucleic acid duplexes is controlled by the denaturation, or "off", rate because the measured duplex formation, or "on", rate constants tend to be similar regardless of sequence.[12] However, this speculation has not yet been rigorously tested.

The base-by-base mechanism first proposed by Wetmur and Davidson[13] is the typical starting point for the interpretation of kinetic data. This mechanism has often been characterized in terms of a nucleation step followed by a fast zipping of the remaining base pairs. The first, rate-determining nucleation step takes single-stranded DNA or RNA to a nucleated duplex with two to four[14−16] H-bonded and stacked bases. Although most sources agree that only a few H-bonded bases exist in the nucleated intermediate, the number of base pairs that must align at the transition state has been estimated by Manning and others to be much higher, 15 or 16 bases.[17−19] This nucleation step is followed by a rapid zipping step in which the rest of the duplex base stacks and hydrogen bonds. Each of these steps most likely consists of individual base-by-base steps that cannot be distinguished and are thus treated as an ensemble or kinetic cluster.[20] In the steady state limit of this model, the nucleated intermediate is not kinetically significant, and this model correlates with the two-state model generally used to obtain thermodynamic parameters from melting data. In this limit, the on and off rate constants can be assigned to the formation and denaturation, respectively, of the nucleation site, which is rate-limiting.

In contrast to the large thermodynamic data set for nucleic acid duplex formation found in the literature, the kinetic data set is much smaller. Whereas most thermodynamic studies have been conducted using the same solvent system (1 M NaCl), the existing kinetic data have been obtained under a variety of solvent conditions, making the correlation of these kinetic data with thermodynamic data difficult. Furthermore, the values of overall thermodynamic parameters do not depend on the detailed molecular mechanism for the reaction, whereas values of measured rate constants do reflect the mechanism. Recently,

Received: September 24, 2012
Revised: January 17, 2013
Published: January 28, 2013

Table 1. Thermodynamic Parameters for Duplex Formation[a]

	average of curve fits				T_M^{-1} vs log C_t plot			
duplex[b]	$-\Delta H^\circ$ (kcal/mol)	ΔS° (cal K^{-1} mol^{-1})	$-\Delta G^\circ_{37}$ (kcal/mol)	T_M[b] (°C)	$-\Delta H^\circ$ (kcal/mol)	$-\Delta S^\circ$ (cal K^{-1} mol^{-1})	$-\Delta G^\circ_{37}$ (kcal/mol)	T_M[b] (°C)
5′ r-CACGGCUC	76	210	13	65.7	80	220	13	65.4
r-GUGCCGAG 5′					80	210	14	68.0
5′ r-CACGGCUC	69	190	9.7	52.0	77	220	10	51.6
d-GTGCCGAG 5′					68	190	10	52.2
5′ r-GAGCCGUG	76	210	9.9	51.4	66	180	9.5	51.4
d-CTCGGCAC 5′					65	180	9.2	52.6
5′ d-CACGGCTC	66	180	9.9	53.7	71	200	10	53.2
d-GTGCCGAG 5′					58	150	9.8	55.7
5′ r-CACAGCAC	90	250	13	60.3	82	220	12	60.0
r-GUGUCGUG 5′					76	200	12	60.2
5′ r-CACAGCAC	67	180	9.5	51.3	62	170	9.2	51.2
d-GTGTCGTG 5′					54	150	8.2	51.1
5′ r-GUGCUGUG	79	230	8.0	42.9	86	250	8.0	42.6
d-CACAGCAC 5′					60	170	7.5	43.1
5′ d-CACAGCAC	64	180	8.7	47.8	65	180	8.6	47.5
d-GTGTCGTG 5′					52	150	8.6	47.7

[a]Solutions are as follows: 1.0 M NaCl, 10 mM sodium cacodylate, and 0.5 mM EDTA (pH 7.0) measured (top row) and predicted as described in the text (bottom row). [b]Calculated at an oligomer concentration of 10^{-4} M.

photon counting histograms (PCH) and fluorescence correlation spectroscopy (FCS) in conjunction with fluorescence resonance energy transfer (FRET) have been used to study hairpin formation below the melting point.[17,21−30] These studies have shown that the formation and/or denaturation of a kinetically important intermediate often contributes to the average rate constant that is measured by ensemble methods such as time-resolved absorbance[13,31−33] or fluorescence,[34−36] nuclear magnetic resonance relaxation,[37] temperature jump,[14−16,36,38−40] or stopped flow.[15,25,29,41] Whether a kinetically important intermediate exists along the path to duplex formation seems to be dependent on sequence and reaction conditions; thus, the overall rate constants reported in the literature often correlate with different sequences of molecular events. These differences in mechanism make the direct comparison of rate constants to each other and to thermodynamic data difficult.

Therefore, in this study, we examine the thermodynamics and kinetics of duplex formation for two sets of oligomers designed to be non-self-complementary and to minimize mismatches or off path intermediate formation. The short length (eight bases) makes hairpin formation as well as other off path intermediates unlikely. Indeed, no homo- or heterodimers with negative changes in free energy at 25 °C in 1 M NaCl buffer are found using Oligo Analyzer version 3.1 on the Integrated DNA Technologies (IDT) website (http://www.idtdna.com). The thermodynamics and kinetics of these two sets of octamers are measured under identical conditions (1 M NaCl) to facilitate comparisons between the thermodynamic and kinetic results. Each set consists of four duplexes, DNA−DNA, RNA−RNA, and the two DNA−RNA hybrids. These data allow us to utilize linear free energy plots to rigorously test the assumption that the off rate controls the relative stability of the nucleic acid duplexes. The success of the linear free energy analysis for this limited data set gives us confidence that this will prove to be a helpful tool for elucidation of common mechanistic elements in nucleic acid folding.

EXPERIMENTAL PROCEDURES

Buffer. All reactions were conducted in a 1 M NaCl, 10 mM cacodylic acid, 0.001 M EDTA (pH 7) buffer solution

Nucleic Acid Solution Preparation. All single-stranded DNA and RNA was purchased from Integrated DNA Technologies (IDT). Purities were checked by analytical thin layer chromatography and were greater than 90%. The lyophilized and desalted oligomers were taken up into water to provide an approximately 200 μM solution. Individual strand concentrations were calculated from high-temperature single-strand absorbance at 260 nm using nearest-neighbor extinction coefficients.[42,43] Stock solutions were stored at −20 °C. From these stock solutions, working solutions at concentrations from 2 to 10 μM were prepared by placing the required amount of stock solution in a microcentrifuge tube and drying. Once dry, the nucleic acid was resuspended in the 1 M NaCl buffer. Working solutions were stored at 4 °C until they were used.

Melting Curve and Data Analysis. Optical melting experiments were performed using a Beckman DU 640 spectrophotometer and high-performance temperature controller at 280 nm. Absorbance changes for oligomers were recorded as a function of temperature at a heating or cooling rate of 1 °C/min as described previously.[44] The thermodynamics derived from the heating and cooling curve gave identical values indicative of an equilibrium system. The experiment was repeated at 10 varying sample concentrations to give an at least 50-fold concentration range (10 μM to 1 mM) for each sample. Absorbance versus temperature profiles were fit to a two-state model with sloping base lines using a nonlinear least-squares program.[45] Thermodynamic parameters for the oligomers were determined from both the average of the individual melt curves and plots of the reciprocal melting temperature (T_M^{-1}) versus $\ln(C_t/4)$ for non-self-complementary sequences.

Stopped-Flow Experiments. The KinTek SF-300X stopped-flow instrument was used to determine the rate of nucleic acid duplex formation of the various strands at varied nucleic acid concentrations and temperatures. A circulating water bath regulated the temperature of the working solutions

dx.doi.org/10.1021/bi3013005 | Biochemistry 2013, 52, 765−772

housed in two separate syringes. Each syringe contained equal concentrations of complementary nucleic acid solutions that were allowed to equilibrate to the desired temperature before the analysis. Analysis of each pair of nucleic acid oligomers was completed at temperatures ranging from 278 to 303 K in approximately 5 K increments. The syringe drive delivered equal volumes (~30 μL) of each solution into the reaction chamber through a rapid mixing chamber. Once the solution was inside the reaction chamber, the absorbance at 280 nm was recorded approximately every 1.5−30 ms (depending on the total time frame of the experiment) with a dead time of approximately 1.5 ms to produce an absorbance versus time kinetic profile.

Prior to analysis, the cell was flushed with at least 4 mL of deionized water. A reference reading was then taken with deionized water. The cell was rinsed with deionized water and re-referenced between each change in nucleic acid solution. Data collection times varied throughout the experiment, ranging from 0.5 to 10 s, to ensure that each profile was collected over five or six half-lives. In each case, 2000 data points were recorded. For each duplex formation reaction, at each temperature, at each nucleic acid concentration, between 12 and 20 injections were taken and averaged. These average kinetic profiles were analyzed using a nonlinear least-squares fit to the integrated second-order rate equation. Second-order rate constants for each nucleic acid concentration were averaged. All error bars represent plus or minus the average deviation about the mean of three to four trials at different nucleic acid concentrations. A second-order fit is consistent with the two-state model as discussed above. This simple model fits our data well as it does a similar kinetic data set obtained by Carillo-Nava.[41] We note that both our kinetic data set and Carillo-Nava's data set were obtained at temperatures well below the melting point of the duplex where the off rate is insignificant compared to the on rate. Thus, no attempt was made to extract the off rate constants from the data by using a model that is more complicated than necessary to fit the data.

RESULTS

The thermodynamic parameters for duplex formation in 1 M NaCl melt buffer for two sets of duplexes are listed in Table 1. Each set consists of four duplexes composed of the RNA−RNA, DNA−DNA, and both RNA−DNA hybrids with identical sequences (U substituted for T in the RNA strands). The sets were selected to vary in GC content from 62 to 75%. For the eight duplexes reported here, the average differences between the ΔG°_{37} and ΔH° values derived from the T_M^{-1} versus $\ln(C_t/4)$ plots and average curve fits are 2.3 and 8.9%, respectively. Using the nearest-neighbor model for duplex formation,[6−9] the stabilities of the duplexes are well predicted, with the average differences between the measured and predicted free energy and melting temperature being 0.3 kcal/mol and 0.8 °C, respectively. As expected, the RNA−RNA duplexes were more stable than either the DNA−DNA or hybrid duplexes that all display similar stabilities.

Kinetic profiles fit well to a second-order integrated rate equation with χ^2 values of $<3 \times 10^{-4}$. All kinetic profiles have been measured at three or four total nucleic acid concentrations (C_t) between 2 and 10 μM. Representative kinetic profiles for three different temperatures for the 5′ r-CACGGCUC/5′ r-GUGCCGAG duplex formation for 6 μM RNA and 1 M NaCl buffer are shown in Figure 1. The symbols represent data points for the average profile of 12−20 injections, and the solid lines

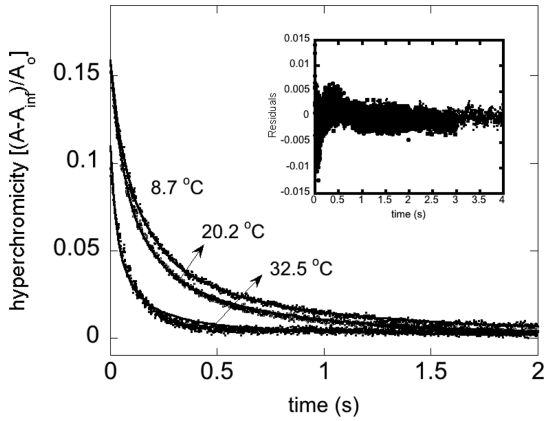

Figure 1. Second-order kinetic profiles for renaturation of the 5′ r-CACGGCUC/5′ r-GUGCCGAG duplex. The concentration of each strand was 6 μM in 10 mM cacodylic acid buffer with 1.0 M NaCl. The hyperchromicity as a function of time for three temperatures (8.7, 20.2, 32.5 °C) is shown. Solid lines through the data points represent the best fit to the integrated second-order rate (eq 1) in the text. Residuals (|data point − fit value|) are shown in the inset.

through the data points are the least-squares best fit to the second-order integrated rate equation shown in eq 1. In eq 1, $A(t)$ is the absorbance at any time, k_{on} is the duplex formation rate constant, C_t is the initial total concentration of nucleic acid oligomers, and t is the time. Fits were obtained using $k_{on}C_t = k_{obs}$, $A(\infty)$, and $\Delta A = A(0) - A(\infty)$ as adjustable parameters.

$$A(t) = A(\infty) + \frac{A(0) - A(\infty)}{1 + k_{on}C_t t} \quad (1)$$

The second-order rate constants (k_{on}) for each temperature investigated are listed in Tables 2 and 3 along with the equilibrium constants for each temperature. Equilibrium constants were calculated from the average change in free energy derived from the melting curves. Errors for the rate constants are estimated using the average error about the mean of three or four measurements at different nucleic acid concentrations. Errors in the equilibrium constants are propagated from the standard deviation about the average values of ΔH and ΔS obtained from fits to the melt curves and fits to plots of T_M^{-1} versus $\ln(C_t/4)$. Second-order rate constants for duplex formation (k_{on}) extracted from these fits were all on the order of 10^6 M^{-1} s^{-1}, in agreement with previous measurements of duplex formation reactions.[14−16,30,38,40,41]

Eyring plots for each data set are shown in panels a (75% GC content sequences) and b (62.5% GC content sequences) of Figure 2. These plots are derived from the transition state theory expression for the rate constant as a function of temperature as shown in eq 2. All plots exhibit negative slopes indicative of positive changes in activation enthalpies. Activation enthalpies derived from these slopes and activation entropies derived from the y-intercepts of these plots are listed in Table 4.

$$k(T) = \frac{\kappa k_B T}{h} e^{\Delta^\ddagger S/R} e^{-\Delta^\ddagger H/RT} \quad (2)$$

where $k(T)$ is the rate constant as a function of temperature, T; κ is the transmission coefficient; k_B is Boltzmann's constant (1.38×10^{-23} J/K); h is Planck's constant (6.626×10^{-34} J s); R is the gas constant (1.987 kcal mol^{-1} K^{-1}); and $\Delta^\ddagger H$ and $\Delta^\ddagger S$

dx.doi.org/10.1021/bi3013005 | Biochemistry 2013, 52, 765−772

Table 2. Rate Constants and Equilibrium Constants for 75% GC Duplex Formation

	5′ r-CACGGCUC		5′ r-CACGGCUC		5′ r-GAGCCGUG		5′ d-CACGGCTC	
	r-GUGCCGAG 5′		d-GTGCCGAG 5′		d-CTCGGCAC 5′		d-GTGCCGAG 5′	
T^a (°C)	$k_{on}{}^b$ (μM^{-1} s^{-1})	K^c ($\times 10^{-8}$)	$k_{on}{}^b$ (μM^{-1} s^{-1})	K^c ($\times 10^{-8}$)	$k_{on}{}^b$ (μM^{-1} s^{-1})	K^c ($\times 10^{-8}$)	$k_{on}{}^b$ (μM^{-1} s^{-1})	K^c ($\times 10^{-8}$)
6.6	2.3	19000000	5.1	39000	2.9	24000	4.4	20000
11.0	3.9	1900000	6.4	5100	5.2	3300	5.4	3000
15.9	5.7	170000	8.2	560	7.3	390	6.5	380
20.1	7.9	22000	9.6	90	14	66	7.0	69
25.3	12	1900	12	10	20	7.9	8.8	8.9
30.6	16	170	14	1.2	26	0.98	10	1.2

[a]Average for measurement of all k values in a given row. [b]All data shown to two significant figures. Average error of ±12%. [c]Calculated from thermodynamic parameters determined from melt data and rounded to two significant figures.

Table 3. Rate Constants and Equilibrium Constants for 62.5% GC Duplex Formation

	5′ r-CACAGCAC		5′ r-CACAGCAC		5′ r-GUGCUGUG		5′ d-CACAGCAC	
	r-GUGUCGUG 5′		d-GTGTCGTG 5′		d-CACGACAC 5′		d-GTGTCGTG 5′	
T^a (°C)	$k_{on}{}^b$ (μM^{-1} s^{-1})	K^c ($\times 10^{-8}$)	$k_{on}{}^b$ (μM^{-1} s^{-1})	K^c ($\times 10^{-8}$)	$k_{on}{}^b$ (μM^{-1} s^{-1})	K^c ($\times 10^{-8}$)	$k_{on}{}^b$ (μM^{-1} s^{-1})	K^c ($\times 10^{-8}$)
6.9	3.5	29000000	3.2	3100	4.4	8300	4.3	1100
10.8	6.9	3500000	4.7	630	4.5	1100	5.3	210
16.3	7.9	190000	6.1	72	6.1	68	5.8	24
20.0	11	2900	6.3	18	6.8	11	7.3	5.9
25.7	16	1800	9.5	2.1	8.3	0.75	11	0.71
30.6	24	170	21	0.37	27	0.080		0.12

[a]Average for measurement of all k values in a given row. [b]All data shown to two significant figures. Average error of ±12%. [c]Calculated from thermodynamic parameters determined from melt data and rounded to two significant figures.

are the differences in enthalpy and entropy, respectively, between the reactants and the transition state.

DISCUSSION

The stability of all of the duplexes investigated here was predicted well by the nearest-neighbor models for the respective helical types. In addition, a simple second-order integrated rate equation was able to fit all kinetic profiles. These results suggest that neither the single-stranded oligomers nor the resulting duplexes formed any unusual secondary structure.

Table 4 displays the values of $\Delta^{\ddagger}H$ and $\Delta^{\ddagger}S$ obtained from the Eyring plots in panels a and b of Figure 2. Values of $\Delta^{\ddagger}S$ are calculated assuming a transmission coefficient (κ in eq 2) of 1. This assumption draws into question the $\Delta^{\ddagger}S$ values. However, given the reasonable assumption that the transmission coefficients for all duplex reactions are approximately the same, the trends in calculated $\Delta^{\ddagger}S$ (and thus $\Delta^{\ddagger}G$) values hold.

The activation parameters listed in Table 4 were used to calculate the change in the free energy of activation for the duplex formation (on) reaction ($\Delta^{\ddagger}G_{on}$) at 298 K. Because the off rate constants could not be extracted from the kinetic profiles, the thermodynamic values listed in Table 1 were used in conjunction with $\Delta^{\ddagger}G_{on}$ to calculate the change in the free energy of activation for the reverse denaturation reaction ($\Delta^{\ddagger}G_{off} = \Delta^{\ddagger}G_{on} + \Delta G^{\circ}_{rxn}$) at 298 K. The filled circles in panels a and b of Figure 3 display the correlations of $\Delta^{\ddagger}G_{off}$ and $\Delta^{\ddagger}G_{on}$ with ΔG°_{rxn} (all at 298 K) from this work. Linear free energy plots, like those in Figure 3, summarize the kinetic and thermodynamic energies for a series of related reactions. Reactions that occur on the same (or similar) potential energy surface are expected to display a linear relationship between the standard free energy and the free energy change of activation.[46] Thus, free energy plots for a series of related reactions can help to elucidate differences in transition state position or differences in the energy landscape for the reaction.[47−55]

Included for comparison in panels a and b of Figure 3 are data from four studies in the literature in which the kinetics and thermodynamics of various sequences were obtained under the same reaction conditions. The study by Chen et al. was designed to investigate the effect of secondary structure in the single strands and was conducted at 0.1 M NaCl.[36] These data are shown in Figure 3 as filled diamonds. Chen's data included a negative $\Delta^{\ddagger}H_{on}$ at high temperatures and a positive $\Delta^{\ddagger}H_{on}$ at low temperatures. The value of $\Delta^{\ddagger}H_{off}$ was positive at all temperatures. Both ranges have been used to calculate $\Delta^{\ddagger}G_{on}$, leading to twice as many filled diamonds in panel b compared to panel a of Figure 3. The study by Porschke et al. was designed to investigate the effect of a GC pair on the thermodynamics and kinetics of duplex formation using nine different sequences, two of which were self-complementary. Porschke's study was conducted at 0.05 M NaCl, and the data are displayed as solid triangles in Figure 3.[56] Williams et al. investigated the self-complementary sequence d-GCATGC at 1 M NaCl.[16] Their data fall on the same trend line as our data also obtained at 1 M NaCl and are shown as a filled square in Figure 3. Finally, Avizonis studied two self-complementary sequences, one with GG mismatches and one with CC mismatches.[37] These data are shown as empty circles in Figure 3.

Linear Relationship for the Denaturation Reaction. Figure 3 suggests three important conclusions about duplex formation. First, all points lie very nearly along the linear trend line described by the data from this work as shown in Figure 3a. We note that all literature values obtained for <1.0 M NaCl (except L0A/TDS and H6A/TDS from Chen et al., both of which have mismatches in the final duplex) lie along a linear trend line that is parallel to the one shown. The larger y-

dx.doi.org/10.1021/bi3013005 | Biochemistry 2013, 52, 765−772

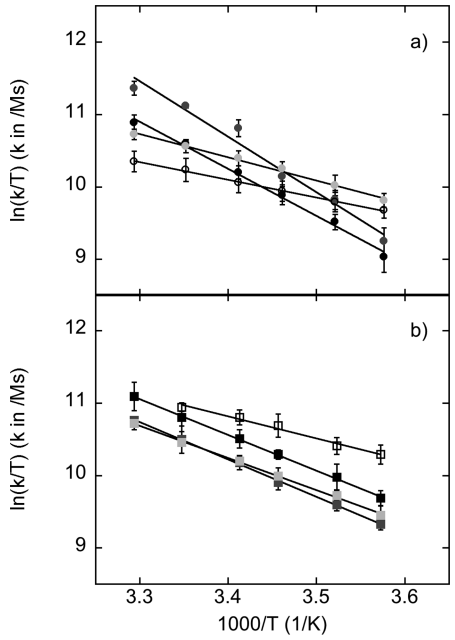

Figure 2. (a) Eyring plots of $\ln(k/T)$ as a function of $1/T$ for the 75% GC content sequences. Points represent the measured rate constant data, and the solid lines are linear least-squares fit to each data set: (black circles) RNA, (white circles) DNA, (dark gray circles) r-CACGGCUC/d-GAGCCGTG, and (light gray circles) r-GAGCC-GUG/dCACGGCTC. Error bars represent the average error about the mean of three or four measurements taken at different nucleic acid concentrations. (b) Eyring plots of $\ln(k/T)$ as a function of $1/T$ for the 62.5% GC content sequences. Points represent the measured rate constant data, and the solid lines are linear least-squares fit to each data set: (black squares) RNA, (white squares) DNA, (dark gray squares) r-GUGCUGUG/d-CACAGCAC, and (light gray squares) r-CACAG-CAC/d-GTGCTGTG. Error bars represent the average error about the mean of three or four measurements taken at different nucleic acid concentrations.

Table 4. Kinetic Parameters for Duplex Formation

duplex	$\Delta^{\ddagger}H_{on}$ (kcal/mol)	$\Delta^{\ddagger}S_{on}$ (cal mol^{-1} K^{-1})
5′ r-CACGGCUC r-GUGCCGAG 5′	12.9 ± 0.6	17 ± 2
5′ r-CACGGCUC d-GTGCCGAG 5′	6.4 ± 0.5	−5 ± 1
5′ r-GAGCCGUG d-CTCGGCAC 5′	15 ± 1	26 ± 4
5′ d-CACGGCTC d-GTGCCGAG 5′	4.8 ± 0.1	−10.6 ± 0.5
5′ r-CACAGCAC r-GUGUCGUG 5′	9.8 ± 0.2	7.1 ± 0.6
5′ r-CACAGCAC d-GTGTCGTG 5′	8.8 ± 0.2	3.2 ± 0.7
5′ r-GUGCUGUG d-CACGACAC 5′	10.3 ± 0.2	8.0 ± 0.6
5′ d-CACAGCAC d-GTGTCGTG 5′	6.1 ± 0.5	−5 ± 2

intercept of this parallel trend is likely the result of the lower-ionic strength conditions under which these reactions were conducted as discussed below. This strong correlation (R^2 = 0.996) suggests that all reactions occur by a common mechanism with a similar transition state structure. Although the correlation between the free energy change for the forward

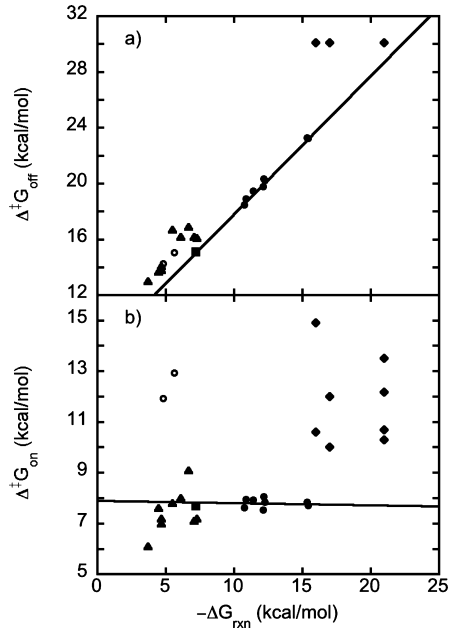

Figure 3. (a) Correlation between the activation free energy for denaturation and the free energy of reaction at 298 K for all duplexes studied in this work and values found in the literature: (●) this work, (■) Williams et al.,[16] (◆) Chen et al.,[36] (▲) Porschke et al.,[40] and (○) Avizonis et al.[37] (b) Correlation between the activation free energy for renaturation and the reaction free energy at 298 K. Symbols are the same as in panel a. Solid lines are linear regression fits to the solid circles. (a) $\Delta^{\ddagger}G_{off} = 7.89 + 0.991\Delta G^{\circ}_{rxn}$; $R^2 = 0.996$. (b) $\Delta^{\ddagger}G_{on} = 7.89 + 0.009\Delta G^{\circ}_{rxn}$; $R^2 = 0.096$.

reaction and the overall free energy change for the same set of reactions is weak (R^2 = 0.1), microscopic reversibility requires that the forward reaction and the reverse reaction go through the same transition state structure. Thus, a linear free energy correlation with either the forward or reverse reaction indicates a common set of molecular events for a series of reactions provided the equilibrium reactions represent elementary steps.[51] The thermodynamic and kinetic data reported here are consistent with a two-state transition, and thus, the forward and reverse reactions can be treated as elementary steps. This then allows us to speculate about the structure of the transition state in the context of the reactant (single-stranded) and product (double-stranded) structures.

Second, the slope value of ∼1 for the correlation with $\Delta^{\ddagger}G_{off}$ shown in Figure 3a indicates a transition state that is more structurally similar to the single strands than to the duplex.[51] In other words, the free energy of activation for denaturation has a 1:1 correspondence with the free energy of reaction, indicating that nearly all the base-stacking and H-bonding interactions that stabilize the duplex are disrupted in the transition state. Thus, the transition state occurs early in the duplex formation (on) reaction and has no H-bonding and little to no base stacking, which was suggested by others.[13,18]

Finally, the *y*-intercept of these plots indicates the "intrinsic" activation free energy for a hypothetical duplex reaction for which the stabilizing forces, such as H-bonds or base stacking, in the duplex are equal to those in the single strands (ΔG°_{25} = 0). This suggests that for the off reaction an activation free energy of ∼7.9 kcal/mol is needed over and above the energy needed to disrupt the H-bonds and enough base-stacking interactions so that the free energy of the "unzipping" double

dx.doi.org/10.1021/bi3013005 | *Biochemistry* 2013, 52, 765−772

strand equals that of the equilibrium single-strand structures. Likewise, for the on reaction, an activation free energy of at least 7.9 kcal/mol is required to form the duplex starting with the single strands. This intrinsic activation free energy is approximately equal to the average free energy of activation measured for all duplex reactions studied here, which was 7.80 ± 0.15 kcal/mol. This follows from the fact that the free energy of activation for the forward duplex formation reaction is relatively constant regardless of the stability of the ensuing duplex. The literature values included in Figure 3 for duplex reactions conducted at lower ionic strengths (0.1 and 0.05 M NaCl) show a parallel trend with a *y*-intercept of approximately 9.6 kcal/mol. This suggests that this intrinsic free energy of activation is a function of the ionic strength and increases as the ionic strength decreases.

We can speculate about the origin of this intrinsic free energy of activation. The single strands in solution exist as an ensemble of random coil structures, all of which likely exhibit some base-stacking interactions. In addition, the single strands are solvated by water and condensed ions. Thus, there are three main interactions that will contribute to a change in free energy as the single strands align to form the transition state structure. First, the disruption of some base-stacking interactions as the random coil structures expand to expose complementary bases will destabilize the solution structure as a result of an increase in enthalpy and entropy.[56,57] Second, the association of the two strands will decrease the entropy. However, as the strands associate, the enthalpy will increase because of greater Coulombic repulsion. Third, the enthalpy penalty due to association will be partially offset by increased level of solvation of ions and water, but the increased level of solvation of the transition state will make the entropy penalty only greater. Thus, overall, the effect of association of the strands coupled to an increased level of solvation is likely to destabilize the transition state relative to the single strands.

As seen in Table 4, the change in the enthalpy of activation is always positive, suggesting that weakened intermolecular interactions (such as base stacking) as the strands uncoil and Coulomb repulsion as the strands associate are the dominant interactions governing the change in the enthalpy of activation. The measured change in the entropy of activation reported in Table 4 is negative for the formation of both DNA sequences and one hybrid sequence and positive for all others. In the cases where the formation of the transition state is driven by entropy ($\Delta^{\ddagger}S > 0$), the "uncoiling" of the single-strand solution structures can be identified as the most important interaction. For cases in which an entropy penalty ($\Delta^{\ddagger}S < 0$) exists, association of the aligning strands plays a more important role. Hence, the overall magnitude of the intrinsic change in the free energy of activation for the on reaction is the result of the balance between electrostatic interactions during association of the strands and disruption of base-stacking interactions as the random-coil single-strand structures expand. We plan to investigate these ideas further in the future.

Moving past the transition state toward the ensuing duplex, adjacent bases begin to stack, and the more compact structure that emerges is likely to attract more condensed ions and water molecules. These stabilizing interactions make up the 7.9 kcal/mol decrease in free energy needed for the ensuing duplex to have the same average free energy as the single-strand ensemble.

CONCLUSIONS

We can draw two major conclusions from these data. First, the data are consistent with a common unstructured transition state. The hypothesis of the unstructured transition state holds for these data regardless of the ensuing duplex type or stability. This conclusion cannot yet be generalized to all nucleic acid duplex reactions regardless of sequence, but given the coincidence of current literature values with our data, we hypothesize that this will prove to be general in the case of two-state reactions in which the rate-limiting step is formation of the duplex.

Second, these data have provided a direct test of the hypothesis that the stability of RNA duplexes relative to DNA and hybrid duplexes is controlled by the rate of denaturation and not the rate of duplex formation. Furthermore, the rate of denaturation is controlled primarily by the free energy penalty for disruption of the same H-bonding and base-stacking interactions that determine the stability contribution of nearest-neighbor base pairs in the nearest-neighbor model. Thus, the linear free energy relationship discussed here underlies the success of the nearest-neighbor model for predicting duplex stability.

AUTHOR INFORMATION

Corresponding Author

*Phone: (814) 332-5329. Fax: (814) 332-2789. E-mail: adeckert@allegheny.edu.

Funding

This work was supported by National Science Foundation Grant MCB-0744631, the Allegheny College Academic Support Fund, and the Paul E. and Mildred L. Hill Fund of Allegheny College.

Notes

The authors declare no competing financial interest.

REFERENCES

(1) Kornberg, A. (2005) *DNA Replication*, 2nd ed., Macmillan, New York.

(2) Crick, F. H. C. (1996) Codon-anticodon pairing: The wobble hypothesis. *J. Mol. Biol. 19*, 548−555.

(3) Zamore, P. D., Tuschl, T., Sharp, P. A., and Bartel, D. P. (2000) RNAi: Double stranded RNA directs the ATP-dependnet cleavage of mRNA at 21 to 23 nculeotide intervals. *Cell 101*, 25−33.

(4) Fire, A., Xu, S., Montgomery, M. K., Driver, S. E., and Mello, C. C. (1998) Potent and specific genetic interference by double stranded RNA in *Caenorhabditis elegans*. *Nature 391*, 806−811.

(5) Vagin, V. V., Sigova, A., Li, C., Seitz, H., Gvozdev, V., and Zamore, P. D. (2006) A distinct small RNA pathway silences selfish genetic elements in the germline. *Science 313*, 320−324.

(6) Santalucia, J. J., Allawi, H. T., and Seneviratne, P. A. (1996) Improved nearest-neighbor parameters for predicting DNA duplex stability. *Biochemistry 35*, 3555−3562.

(7) Xia, T., SantaLucia, J. J., Burkard, M. E., Kierzek, R., Schroeder, S. J., Jiao, X., Cox, C., and Turner, D. H. (1998) Thermodynamic parameters for an expanded nearest-neighbor model for formation of RNA duplexes with Watson-Crick base pairs. *Biochemistry 37*, 14719−14735.

(8) Sugimoto, N., Nakano, S., Katoh, M., Matsumura, A., Nakamuta, H., Ohmich, T., Yoneyama, M., and Sasaki, M. (1995) Thermodynamic parameters to predict stability of RNA/DNA hybrid duplexes. *Biochemistry 34*, 11211−11216.

(9) Sugimoto, N., Nakano, S., Yoneyama, M., and Handa, K. (1996) Improved thermodynamic parameters and helix initiation factor to predict stability of DNA duplexes. *Nucleic Acids Res. 24*, 4501−4505.

(10) Turner, D. H., Sugimoto, N., and Freier, S. M. (1988) *Annu. Rev. Biophys. Chem. 17*, 167−192.
(11) Xia, T., Mathews, D. H., and Turner, D. H. (2001) in *RNA: Life's Indispensable Molecule* (Soll, D. G., Nishimura, S., and Moore, P. B., Eds.) pp 21−48, Elsevier, Amsterdam.
(12) Bloomfield, V. A., Crothers, D. M., and Tinoco, I. J. (2000) *Nucleic Acids: Structures, Properties and Functions*, University Science Books, Sausalito, CA.
(13) Wetmur, J. G., and Davidson, N. (1968) Kinetics of renaturation of DNA. *J. Mol. Biol. 31*, 349−370.
(14) Craig, M. E., Crothers, D. M., and Doty, P. (1971) Relaxation kinetics of dimer formation by self complementary oligonucleotides. *J. Mol. Biol. 68*, 383−401.
(15) Porschke, D., and Eigen, M. (1971) Co-operative non-enzymatic base recognition. III. Kinetics of the helix-coil transition of the oligoribouridylic-oligoriboadenylic acid system and of oligoriboadenylic acid alone at acidic pH. *J. Mol. Biol. 62*, 361−381.
(16) Williams, A. P., Longfellow, C. E., Freier, S. M., Kierzek, R., and Turner, D. H. (1989) Laser temperature-jump, spectroscopic, and thermodynamic study of salt effects on duplex formation by dGCATGC. *Biochemistry 28*, 4283−4291.
(17) Kim, J., Doose, S., Neuweiler, H., and Sauer, M. (2006) The initial step of DNA hairpin folding: A kinetic analysis using fluorescence correlation spectroscopy. *Nucleic Acids Res. 34*, 2516−2527.
(18) Manning, G. S. (1976) On the application of polyeletroyte limiting laws to the helix-coil transition of DNA. V. Ionic effects on renaturation kinetics. *Biopolymers 15*, 1333−1343.
(19) Sikorav, J., Orland, H., and Braslau, A. (2009) Mechanism of thermal renaturation and hybridization of nucleic acids: Kramers process and universality in Watson-Crick base pairing. *J. Phys. Chem. B 113*, 3715−3725.
(20) Zhang, W., and Chen, S. (2006) Exploring the complex folding kinetics of RNA hairpins: I. General folding kinetics analysis. *Biophys. J. 90*, 765−777.
(21) Bonnet, G., Krichevsky, O., and Libchaber, A. (1998) Kinetics of conformational fluctuations in DNA hairpin-loops. *Proc. Natl. Acad. Sci. U.S.A. 95*, 8602−8606.
(22) Jung, J., and Orden, A. V. (2006) A three-state mechanism for DNA hairpin folding characterized by multiparameter fluorescence fluctuation spectroscopy. *J. Am. Chem. Soc. 128*, 1240−1249.
(23) Grunwell, J. R., Glass, J. L., Lacoste, T. D., Deniz, A. A., Chemla, D. S., and Schultz, P. G. (2001) Monitoring the conformational fluctuations of DNA hairpins using single-pair fluorescence resonance energy transfer. *J. Am. Chem. Soc. 123*, 4295−4303.
(24) Bowman, G. R., Huang, X., Yao, Y., Sun, J., Carlsson, G., Guibas, L. J., and Pande, V. S. (2008) Structural insight into RNA hairpin folding intermediates. *J. Am. Chem. Soc. 130*, 9676−9678.
(25) Zuo, E. T., Tanious, F. A., Wilson, W. D., Zon, G., Tan, G., and Wartell, R. M. (1990) Effect of base-pair sequence on the conformations and thermally induced transitions in oligodeoxyribonucleotides containing only AT base pairs. *Biochemistry 29*, 4446−4456.
(26) Yin, Y., and Zhao, X. S. (2011) Kinetics and dynamics of DNA hybridization. *Acc. Chem. Res. 44*, 1172−1181.
(27) Jung, J., Ihly, R., Scott, E., Yu, M., and Orden, A. V. (2008) Probing the complete folding trajectory of a DNA hairpin using dual beam fluorescence fluctuation spectroscopy. *J. Phys. Chem. B 112*, 127−133.
(28) Wallace, M. I., Ying, L., Balasubramanian, S., and Klenerman, D. (2001) Non-Arrhenius kinetics for the loop closure of a DNA hairpin. *Proc. Natl. Acad. Sci. U.S.A. 98*, 5584−5589.
(29) Nayak, R. K., Peersen, O. B., Hall, K. B., and Van Orden, A. (2012) Millisecond time-scale folding and unfolding of DNA hairpins using rapid-mixing stopped-flow kinetics. *J. Am. Chem. Soc. 134*, 2453−2456.
(30) Chen, X., Zhou, Y., Qu, P., and Zhao, X. S. (2008) Base-by-base dynamics in DNA hybridization probed by fluorescence correlation spectroscopy. *J. Am. Chem. Soc. 130*, 16947−16952.
(31) Subrirana, J. A., and Doty, P. (1966) Kinetics of renaturation of denatured DNA. I. Spectophotometric results. *Biopolymers 4*, 171−187.
(32) Record, J. M. T. (1972) Kinetics of helix-coil transition in DNA. *Biopolymers 11*, 1435−1484.
(33) Gao, Y., Wolf, L. K., and Georgiadis, R. M. (2006) Secondary strucutre effects on DNA hybridization kinetics: A solution versus surface comparison. *Nucleic Acids Res. 34*, 3370−3377.
(34) Genot, A. J., Zhang, D. Y., Bath, J., and Turberfield, A. J. (2011) Remote toehold: A mechanism for flexible control of DNA hybridization kinetics. *J. Am. Chem. Soc. 133*, 2177−2182.
(35) Kim, J., and Shin, J. (2010) Probing the transition state for nucleic acid hybridization using ϕ-value analysis. *Biochemistry 49*, 3420−3426.
(36) Chen, C., Wang, W., Wang, Z., Wei, F., and Zhao, X. S. (2007) Influence of secondary structure on kinetics and reaction mechanism of DNA hybridization. *Nucleic Acids Res. 35*, 2875−2884.
(37) Avizonis, D. Z., and Kearns, D. R. (1995) Kinetic and thermodynamic characterization of DNA duplex-hairpin interconversion for two DNA decamers: d(CAACGGGTTG) and d(CAACCCGTTG). *Biopolymers 35*, 187−200.
(38) Nelson, J. W., and Tinoco, I. J. (1982) Comparison of the kinetics of ribo-, deoxyribo- and hybrid oligonucleotide double-strand formation by temperature-jump kinetics. *Biochemistry 21*, 5289−5292.
(39) Ansari, A., and Kuznetsov, S. V. (2005) Is hairpin formation in single-stranded polynucleotide diffusion-controlled? *J. Phys. Chem. B 109*, 12982−12989.
(40) Porschke, D., Uhlenbeck, O. C., and Martin, F. H. (1973) Thermodynamics and kinetics of the helix-coil transition for oligomers containing GC base pairs. *Biopolymers 12*, 1313−1335.
(41) Carrillo-Nava, E., Mejia-Radillo, Y., and Hinz, H. J. (2008) Dodecamer DNA duplex formation is characterized by second-order kinetics, positive activation energies, and a dependence on sequence and Mg^{2+} ion concentration. *Biochemisty 47*, 13153−13157.
(42) Borer, P. N. (1975) in *Handbook of Biochemistry and Molecular Biology: Nucleic Acids* (Fasman, G. D., Ed.) p 589, CRC Press, Cleveland, OH.
(43) Richards, E. G. (1975) in *Handbook of Biochemistry and Molecular Biology: Nucleic Acids* (Fasman, G. D., Ed.) p 197, CRC Press, Clevelenad, OH.
(44) Serra, M. J., Axenson, T. J., and Turner, D. H. (1994) A model for the stabilities of RNA hairpins based on a study of the sequence dependence of stability for hairpins of six nucleotides. *Biochemistry 33*, 14289−14296.
(45) McDowell, J. A., and Turner, D. H. (1996) Investigation of the structural basis for thermodynamic stabilities of tandem GU mismatches: Solution structure of $(rGAGGUCUC)_2$ by two-dimensional NMR and simulated annealing. *Biochemistry 35*, 14077−14089.
(46) Hill, T. L. (1975) Free energy and the kinetics of biochemical diagrams, including active transport. *Biochemistry 14*, 2127−2137.
(47) Aaqvist, J., and Warshel, A. (1990) Free energy relationships in metalloenzyme-catalyzed reactions. Calculations of the effects of metal ion substitutions in staphylococcal nuclease. *J. Am. Chem. Soc. 112*, 2860−2868.
(48) Bjelic, S., and Aaqvist, J. (2006) Catalysis and linear free energy relationships in aspartic proteases. *Biochemistry 45*, 7709−7723.
(49) Hausheer, F. H., Rao, B. G., Saxe, J. D., and Singh, U. C. (1992) Physicochemical properties of (R)- vs (S)-methylphosphonate substitution on antisense DNA hybridization determined by free energy perturbation and molecular dynamics. *J. Am. Chem. Soc. 114*, 3201−3206.
(50) Joris, L., Mitsky, J., and Taft, R. W. (1972) Effects of polar aprotic solvents on linear free-energy relations in hydrogen-bonded complex formation. *J. Am. Chem. Soc. 94*, 3438−3442.
(51) Prakash, M. K. (2011) Insights on the role of (dis)order from protein-protein interaction linear free-energy relationships. *J. Am. Chem. Soc. 133*, 9976−9979.
(52) Quinn, D. M., Feaster, S. R., Nair, H. K., Baker, N. A., Radic, Z., and Taylor, P. (2000) Delineation and decomposition of energies

involved in quaternary ammonium binding in the active site of acetylcholinesterase. *J. Am. Chem. Soc. 122*, 2975−2980.
(53) Smithrud, D. B., and Diederich, F. (1990) Strength of molecular complexation of apolar solutes in water and in organic solvents is predictable by linear free energy relationships: A general model for solvation effects on apolar binding. *J. Am. Chem. Soc. 112*, 339−343.
(54) Thorson, J. S., Chapman, E., Murphy, E. C., Schultz, P. G., and Judice, J. K. (1995) Linear free energy analysis of hydrogen bonding in proteins. *J. Am. Chem. Soc. 117*, 1157−1158.
(55) Warshel, A., Schweins, T., and Fothergill, M. (1994) Linear free energy relationships in enzymes. Theoretical analysis of the reaction of tyrosyl-tRNA synthetase. *J. Am. Chem. Soc. 116*, 8437−8442.
(56) Pörschke, D., and Eggers, F. (1972) Thermodynamics and kinetics of base-stacking interactions. *Eur. J. Biochem. 26*, 490−498.
(57) Pörschke, D. (1973) The dynamics of nucleic-acid single-strand conformation changes. *Eur. J. Biochem. 39*, 117−126.